1   **Supplementary Information**

2 **Entry and passage behavior of biological cells in a constricted compliant**
3 **microchannel**

4   A. Raj, A. K. Sen[*]

5   Department of Mechanical Engineering, Indian Institute of Technology Madras, Chennai-600036, India
6
7   [*]Author to whom correspondence should be addressed. Email: ashis@iitm.ac.in
8

9
10   **S.1 Theoretical model: total flow rate through constriction with a single cell**

11   In the present work, the cell sample is infused through the micro-constriction device by maintaining the constant pressure
12   across the micro-constriction. Once a single cell enters the micro-constriction, the hydrodynamic resistance of the
13   microchannel changes and the flow rate through the device gets modified accordingly. In this section, we will be discussing
14   the development of a theoretical model to find out the leak flow through the annular region between cell wall and the
15   channel's internal wall by utilizing the deformation profile and the velocity of the cell. This will allow us to find out the
16   total flow rate through the device at a known applied pressure gradient.

17   We take following assumptions for the modelling. The deformed cross-section of the cell in the micro-constriction is
18   assumed to circular. Also, there is always a lubricating layer (of thickness on the order of few hundreds of nm) in the
19   annular region between the cell wall and channel's internal wall [1]. Thus, assuming the micro-constriction to be circular in
20   cross-section, the physical domain is considered as a cylindrical pellet moving through a cylindrical pipette.

21   Further, we find out the velocity profile in the annular region between cell and the wall. Navier-Stokes equation for an
22   incompressible flow in an annular axisymmetric region around the cell (at section BB in Fig. 1(c) of manuscript) with the
23   assumption of fully developed flow and negligible body force, is given as [2]

24
$$\frac{1}{r}\frac{\partial}{\partial r}\left(r\frac{\partial u}{\partial r}\right) = \frac{1}{\mu_m}\left(\frac{\partial p}{\partial z}\right) \tag{1}$$

25   where p is the fluid pressure, u is the flow velocity, and r and z are the radial and axial coordinates, respectively, μ_m is the
26   viscosity of the suspending media.
27
28   Now, the velocity profile in the annular region between the cell and wall is obtained by solving eqn.1 with the boundary
29   conditions $u(r = r_c) = U_c$ (cell velocity) and $u(r = a) = 0$, which yields us the following expression.

30
$$u = \left(\frac{k}{4\mu_m}\right)r^2 + C_1 \ln r + C_2$$

31   where, $C_1 = \dfrac{\left(\dfrac{k}{4\mu_m}\right)\left(a^2 - r_c^2\right) + U_c}{\ln\left(\dfrac{r_c}{a}\right)}$ and, $C_2 = \dfrac{U_c \ln a + \dfrac{k}{4\mu_m}\left(a^2 \ln r_c - r_c^2 \ln a\right)}{\ln\left(\dfrac{a}{r_c}\right)}$ (2)

32   The volume conservation at the section BB (see Fig. 1(c) of manuscript) relates the leak flow Q_{leak} with the velocity profile
33   as follows:

34
$$\int_{r_c}^{a} (2\pi r u)\, dr = Q_{leak} \tag{3}$$

1 Incorporating the velocity profile from equation 2, the above equation yields the expression for Q_{leak} as shown in the Eqn.4.

2
$$\frac{k}{16\mu_m}\left(a^4 - r_c^4\right) + \left\{\frac{2\left(a^2 \ln a - r_c^2 \ln r_c\right) - \left(a^2 - r_c^2\right)}{4}\right\}\left[\frac{\left(\frac{k}{4\mu}\right)\left(a^2 - r_c^2\right) + U_c}{\ln\left(\frac{r_c}{a}\right)}\right] + \left(\frac{a^2 - r_c^2}{2}\right)\left[\frac{U_c \ln a + \frac{k}{4\mu}\left(a^2 \ln r_c - r_c^2 \ln a\right)}{\ln\left(\frac{a}{r_c}\right)}\right] = \frac{Q_{leak}}{2\pi} \quad (4)$$

3 Further, on applying the volume conservation between the inlet flow (at Section AA) and the flow at the cell section (at
4 Section BB) (Fig. 1(c) of manuscript), we get

5
$$Q_{total} = \pi a^2 U_T = Q_{leak} + \pi r_c^2 U_c \quad (5)$$

6 Now, by assuming the leak flow around the cell as flow through a porous structure, the superficial velocity of the sample in
7 the microchannel U_T is related with the average velocity of the flow U_{avg} in the annular region between cell and the wall as

8 $U_T = \varepsilon U_{avg}$[3]. Here, ε is porosity or void fraction and can be found as $\varepsilon = \frac{V_{region} - V_c}{V_{region}}$, where V_{region} is the volume of the
9 region 2 (shown in Fig. 2(a) of manuscript) and V_c is the volume of the cell which can be calculated in terms of deformed
10 radius of the cell r_c and deformed length of a cell l (measured from the experimental microscopic images). Further, the

11 U_{avg} is related to the leak flow rate Q_{leak} as $U_{avg} = \frac{Q_{leak}}{4a^2 - \pi r_c^2}$. Hence U_T can be expressed in terms of Q_{leak} as

12
$$U_T = \varepsilon\left[\frac{Q_{leak}}{4a^2 - \pi r_c^2}\right] \quad (6)$$

13 By combining eqn. 5 and 6 and manipulating, Q_{leak} is represented in terms of r_c as

14
$$Q_{leak} = \left[\frac{\pi r_c^2 U_c\left(4a^2 - \pi r_c^2\right)}{a^2\left(\pi\varepsilon - 1\right) + \pi r_c^2}\right] \quad (7)$$

15 Further, replacing the expression for Q_{leak} from eqn. 7 into eqn. 4, we obtain the relation between r_c and k as follows,

16
$$\frac{r_c^2\left(4a^2 - \pi r_c^2\right)U_c}{2\left\{a^2\left(\pi\varepsilon - 1\right) + \pi r_c^2\right\}} - \frac{\frac{k}{4\mu_m}\left(a^2 - r_c^2\right) + U_c}{4\ln(r_c/a)}\left[2\left(a^2 \ln a - r_c^2 \ln r_c\right) - \left(a^2 - r_c^2\right)\right] - \frac{U_c \ln a + \frac{k}{4\mu}\left(a^2 \ln r_c - r_c^2 \ln a\right)}{2\ln(a/r_c)}\left(a^2 - r_c^2\right) = \frac{k\left(a^4 - r_c^4\right)}{16\mu_m}$$

17 $\quad (8)$

18 The velocity U_c is measured from the experimental high-speed imaging videos. With all other parameters known, the eqn. 8
19 is solved in MATLAB to determine the deformed cell size r_c. Once r_c is known, Q_{leak} can be calculated using Eqn. 7.

20 Now, on coupling eqn. 5 and 7, we find out the total flow rate through the device Q_{total} as shown in the equation 9.

21
$$Q_{total} = \pi r_c^2 U_c\left[1 + \frac{\left(4(a)^2 - \pi r_c^2\right)}{(a)^2\left(\pi\varepsilon - 1\right) + \pi r_c^2}\right] \quad (9)$$

22 The equation 9 is valid for rigid as well as compliant microchannel with $2a$ as the effective hydraulic diameter.

23 **S.2 Device Fabrication**

24 We have fabricated the microfluidic device using photolithography and soft lithography process. The silicon master
25 fabricated using photolithography process was molded to get a PDMS layer containing the microchannel. A detailed
26 description of the device fabrication procedure is explained below. First, a flexi mask designed in AutoCAD LT 2008 and
27 printed at 40000 dpi (Fine Line imaging, USA) was utilized. Then, a 4" silicon wafer (Semiconductor Technology and

1   Application, Milpitas, USA) was pre-processed by cleaning with HF, DI water rinse and followed by baking in oven for 2
2   min at 120º C to remove moisture. Next, to create a photoresist layer, the wafer was spun coated with photoresist SU8-10
3   (Micro Chem Corp, Newton, USA) at 3000 rpm for 30 s with an acceleration of 300 rpm/s and further soft baked at 65º C
4   for 5 min followed by 95º C for 5 min. The resist coated wafer was exposed to UV light (J500IR/VISIBLE, MA6/BA6
5   Semi-Automatic Mask Aligner, Suss Microtec, Germany) through the mask for 9 s. This was followed by a post exposure
6   bake at 65º C for 1 min and 95º C for 2 min, successively. Further, we develop the UV-exposed wafer for 3 min with SU8
7   developer and create the SU8 pattern on top of silicon master. At the end, we place the wafer in oven at 100º C for 30 min
8   which further improves adhesion between photoresist and wafer. Fig.S1(a) shows the microscopic image of the fabricated
9   Si-master.

10   Once the silicon master is ready, PDMS monomer and curing agent (sylgard-184, Silicone Elastomer kit, Dow corning,
11   USA) mixed at mixing ratio 10:1, was poured onto the Si-master after degassifying in the desiccator. Then we cure it inside
12   a vacuum oven at 80º C for 45 min. The cured and hardened PDMS layer containing the channel structure was peeled off
13   the silicon master and cut to size. Then, fluidic access holes for the inlet and the outlet were punched using a 1.5 mm biopsy
14   punch (shoney Scientific, Pondicherry, India). To complete the channel of the device, PDMS layer containing channel was
15   bonded to a glass slide or thin PDMS membrane using oxygen-plasma bonding (Harrick Plasma, Brindley St., USA) in
16   order to fabricate rigid and compliant micro-constriction device respectively. Finally, PTFE tubings (Instech Laboratories,
17   PA, USA) were glued to the access holes to establish fluidic connection.

18   For fabrication of thin PDMS membrane, we have used the following procedure. To increase the flexibility of thin PDMS
19   membrane, we have added 20 % hexane to the prepared PDMS monomer and curing agent (with 10:1 ratio) mixture[4]. Then,
20   this mixture was spin coated over a poly (methyl methacrylate) (PMMA) sheets of size $10 \times 5 \times 0.3$ cm at 2500 rpm for 85 s
21   at an acceleration of 8 rpm/s. Further, the spin coated PMMA sheet was cured inside the vacuum oven at $65^o\,C$ for 6 hours.
22   Once the thin PDMS layer is cured, it is bonded with the PDMS layer containig the microchannel and the PMMA layer is
23   peeled off such that the thin PDMS layer forms one of the walls of the micro-constriction. Using this protocol, we could
24   achieve wall thickness of $22 \pm 2\ \mu m$ and $18.5 \pm 2\ \mu m$, whose young's modulus is determined[4] to be $1.842\ Pa$.

25   The Young's modulus of the thin PDMS membrane used in the current study is $\sim 1\ Mpa$, which compares well with the
26   elasticity modulus values for blood vessels that fall in the wall range of $0.2 - 6.0$ MPa[5]. Thus, a blood vessel of equivalent
27   dimension as the rectangular channel used in the present study would yield comparable values of f_p.
28

29   The two f_p values $f_{p1} = 2.22 \times 10^{-9}\ Pa^{-1}$ and $f_{p2} = 2.64 \times 10^{-9}\ Pa^{-1}$ were arrived at, by changing the thickness of
30   the membrane wall. For a microconstriction of dimension $10.5\ \mu m \times 10.5\ \mu m$, a thin membrane (with $v_m = 0.5$ and
31   $E_m = 1.84\ Mpa$) of thickness $t_{m1} = 22\ \mu m$ and $t_{m2} = 18.5\ \mu m$ yields $f_{p1} = 2.22 \times 10^{-9}\ Pa^{-1}$ and
32   $f_{p2} = 2.64 \times 10^{-9}\ Pa^{-1}$, respectively.

### 33 S.3 Cell culture Protocol

34   The cell lines were purchased from NCCS (National Centre for Cell Sciences, Pune, India). The cell lines kept at -80 ^{o}C
35   were revived and cultured into T-25 flask in Dulbecco's Modified Eagle Medium (DMEM) (Himedia, India), which
36   contained 20% fetal bovine serum and antibiotic mix (50 mg gentamicin, 100 mg streptomycin, and 62.77 mg penicillin),
37   and were incubated in CO_2 incubator. Once the cells were grown to 70 % confluence, the media was removed and the cells
38   were washed three times with Phosphate Buffered Saline. Then, PBS was removed completely and cells were trypsinized
39   with 1X trypsin and incubated for 2-3 min in CO_2 incubator. The trypsinized cells were added with 3.0 mL DMEM to
40   nullify the effect of trypsin on the cells. Then the cell suspension was transferred into 15 mL Falcon tube and centrifuged
41   for 5 min at 1800 rpm. After centrifugation, the supernatant was removed and 1.0 mL of fresh media was added to the
42   pellet. Then, the cells were gently resuspended. 1% Pluronic, BASF was then added to the cell suspension before infusing
43   into the microfluidic device to reduce the adhesion between cells and cell-wall interaction.

44 S.4 Experimental setup and procedure

1   Fig. S1 (a) shows a schematic of the experimental setup. The MFCS-EZ pressure based flow-controller system and the
2   MAESFLO software (Fluigent, Paris, France) constant pressure based flow controller system can infuse the cell sample into
3   the microfluidic device at a pressure resolution of 1 mbar. To avoid any unspecific cell adhesion onto the channel walls, we
4   have coated the microfluidic device with a solution of 1 % Pluronic (BASF, Sigma –Aldrich, USA) with PBS (phosphate-
5   buffered Saline, Germany, Sigma Aldrich). Then, the cell suspension (2×10^5 cells per mL of media with 1% Pluronic,
6   BASF) was infused into the device at constant known pressure. The movement of the cell through the micro-constriction
7   was observed and captured using Inverted microscope (Carl Zeiss Axiovert A1) coupled with a high-speed camera
8   (FASTCAM SA3 model, Photron USA, Inc.) interfaced with PC via Photron Fastcam Viewer 3 software (PFV3). We have
9   used 40X magnification objectives for our experiments. The Cell passage videos were recorded at 4000 frames per second
10 (fps) with the resolution of 256×512 pixels. With a 20X objective the field of view was approximately 0.5 mm.

11
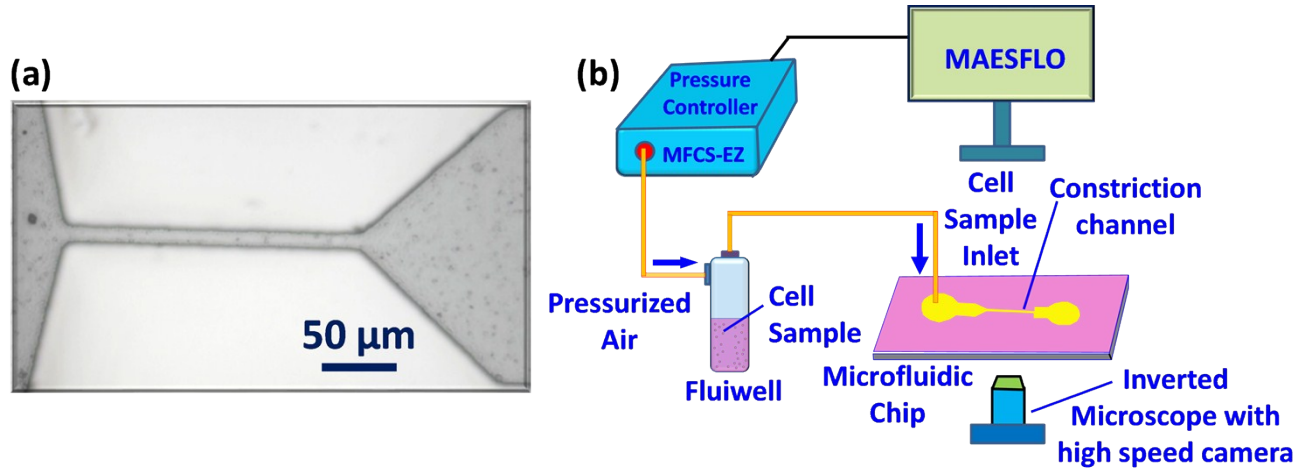
12

13 **Fig. S1** (a) Microscopic image of the single constriction silicon master (b) Schematic of the experimental setup.

14

15 **S.5 Image analysis & Data extraction**

16 We have used Photon FASTCAM Analysis (PFA) software (Motion Analysis Software Version 1.3.2.0, Photron USA, Inc.)
17 to analyse the captured cell passage videos. This software can track the movement of the cell surface (or any interface
18 assigned) and plot the cell position along the length of the microchannel with time. Further, the same plot is utilized to
19 obtain the instantaneous velocity of the cell. The detailed procedure of the image analysis is explained below. Fig. S.2
20 shows the protocol for the image analysis. PFA software can monitor an assigned cell surface (leading edge in the case of
21 entry time analysis and rear edge in the case of transit behaviour analysis) and plot the graphs automatically.

22 First, we measure the diameter of the cell in the upstream before entering the constriction channel by fitting a circle as
23 shown by the dotted green circle (topmost image of Fig. S.2(a)). We have taken 5 measurements for each cell to get a more
24 accurate data. Now, for entry time measurements, we have tracked the leading edge of the cell and noted down its
25 movement into the constriction with time such that $L_p(t_i)$ is the protrusion length of the cell at time instant t_i (see Fig. S.2
26 (a)). When cell completely squeezes into the constriction with maximum protrusion length $L_p(t_e)$, the time is noted down as
27 the entry time t_e of the cell. Also, $L_p(t = t_e)$ was utilized to find out the extension ratio of the cell. Further, for cell transit
28 analysis, we have tracked the rear edge of the cell with time as shown in Fig. S.2(b). The initial edge of the constriction was
29 taken as reference $Z_c(t = 0) = 0$ and Position of the cell $Z_c(t = t_i)$ was noted down after each millisecond and plotted with
30 time, which was also utilized to the find out the instantaneous velocity of cell along the micro-constriction.
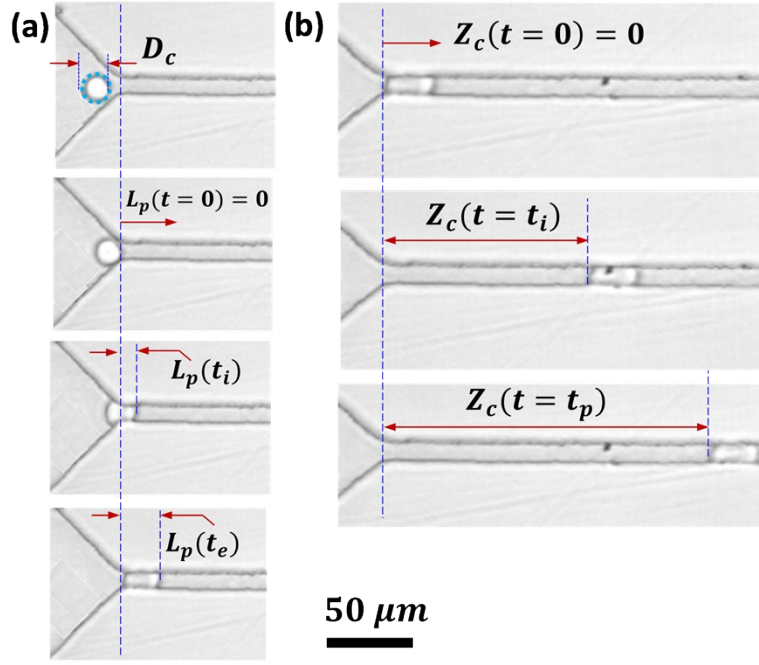
1

2 **Fig. S2** Protocol for image analysis of (a) entry process of the single cell (b) Transit Process of the single cell.

3 **S.5 Experimental results of entry and transit of MDA-MB-231 cell line**

4 In addition to HeLa cell lines (results explained in the main manuscript), we have also investigated the entry and transit
5 behaviour of the MDA-MB-231 cell line through compliant micro-constrictions (with compliance parameters $f_{p0}, f_{p1} \& f_{p2}$)
6 and compared with the same through rigid micro-constrictions. Fig. S3 (a) shows the entry behaviour of a single MDA-
7 MB-231 cell of diameter $18 \pm 0.5\ \mu m$ through micro-constrictions of various flexibilities ($f_{p0}, f_{p1} \& f_{p2}$). Similar to the
8 phenomena observed for HeLa cell line, the contraction zone (Zone II as shown between points
9 $A_m \& B_m, C_m \& D_m\ and\ E_m \& F_m$) of the cell entry is smaller as the flexibility of constriction increases and becomes a
10 single point for f_{p2} as shown by points $E_m \& F_m$. This gives rise to a lower overall entry time for compliant micro-
11 constrictions as shown in Fig. S3 (b). Entry time decreases nearly to half for f_{p1} and to one fourth for f_{p2} compared to rigid
12 microchannel (f_{p0}).

13 Also, the average transit velocity of the MDA-MB-231 cells increases to double for compliant micro-constriction f_{p1}. This
14 phenomenon can be attributed to the fact that the total force response from the cell due to stiffness F_s and viscous damping
15 F_d is dampened on the case of compliant micro-constriction compared to rigid micro-constriction because of the ability of
16 the compliant wall to absorb the excess stress. This reduces the viscous drag on the cell surface and thus the overall cell
17 velocity is increased at same applied pressure gradient. However, there is a limit to this deformation of the thin wall and it
18 does not increase further above a particular compliance parameter as explained in our previous work in more detail[6] (please
19 see Fig.9(b) of our previous work[6]). This is the reason why we see no further rise in velocity for the case of MDA-MB-231
20 cells and there is insignificant increase in the average velocity with the increase in compliance parameter from f_{p1} to f_{p2}.

21 Next, we compare the present experimental data for the transit velocity with that reported by Toner et al. (2016). Toner et al.
22 (2016)[7] have experimentally measured the transit velocity of MDAMB231 cell line through a microconstriction of
23 dimensions $10\mu m \times 10\ \mu m$ (similar to the dimensions used in the current work) and have reported the transit velocity of
24 ~3000 $\mu m/s$, which compares well with the value reported by us $\sim 5000\ \mu m/s$ at a size ratio of 1.8. The differences in the
25 values can be attributed to the biological heterogeneity as well as the experimental conditions.
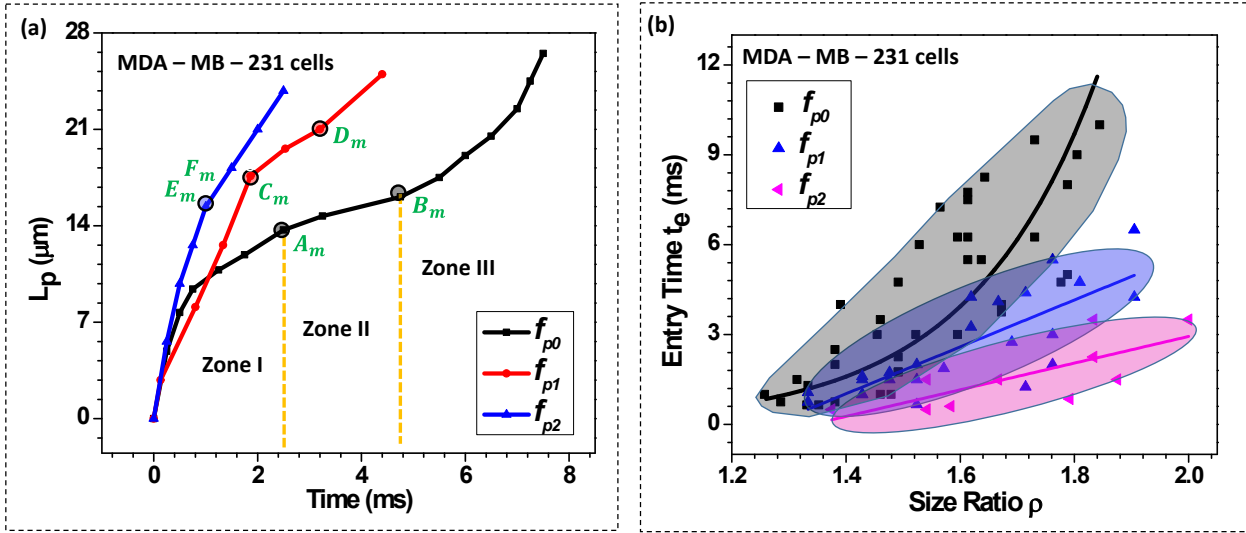
1

2 **Fig. S3** (a) Entry behaviour of a single MDA-MB-231 cell (Diameter $18 \pm 0.5\ \mu m$) through micro-constrictions (Effective
3 hydraulic diameter $10.5 \pm 0.25\ \mu m$) of various flexibilities (b) Comparison of entry time of the MDA-MB-231 cell line
4 through micro-constriction of various flexibilities, applied pressure gradient across the micro-constriction is $100\ mbar$.

5 Further, we have predicted the induced hydrodynamic resistance offered by single MDA-MB-231 cell while migrating
6 through rigid and compliant micro-constrictions (using eqn. 5 of the manuscript as explained in the section 5.3 of the
7 manuscript). The predicted values for MDA-MB-231 cell line show that induced hydrodynamic resistance decreases by
8 nearly three time for compliant micro-constriction (at $\rho = 1.82$) compared to the rigid one. This phenomenon can be
9 attributed to the decrease in the viscous drag acting on the cell surface with the increase in the flexibility of the micro-
10 constriction.
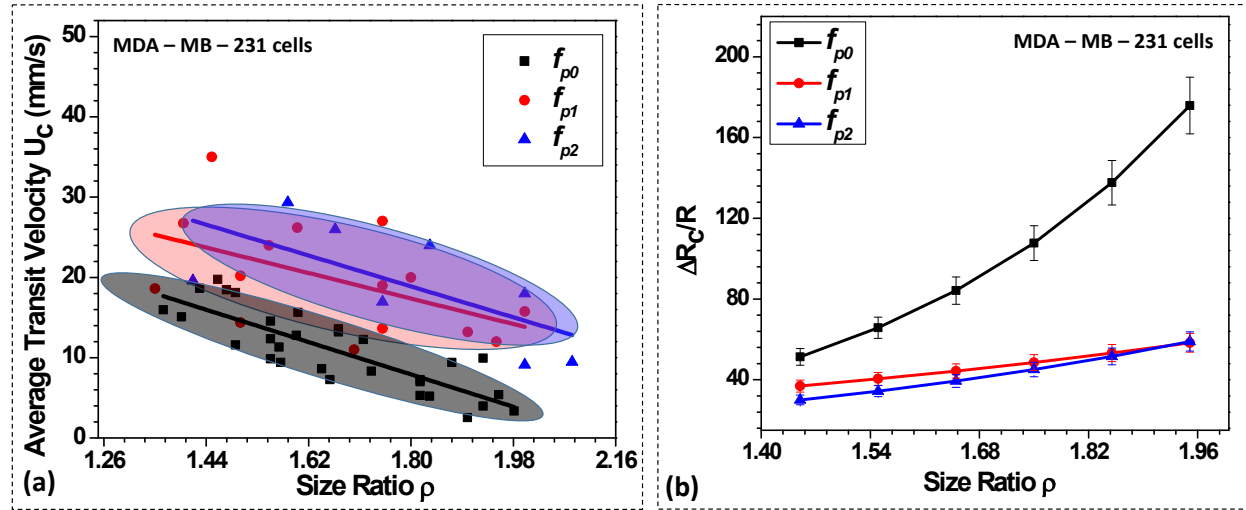
11

12 **Fig. S4** (a) Variation of average transit velocity with the compliance parameter f_p (b) Variation in the induced
13 hydrodynamic resistance $\Delta R_c/R$ (predicted using eqn. 5 of the main manuscript) of HeLa cell with size ratio ρ flowing
14 through micro-constrictions of different compliances (f_{p0}, f_{p1} and f_{p2}) at an inlet pressure of 100 mbar.

15 **S.6 Effect of the cell stiffness over the entry time**

16 Here, we compare the entry time for two different cell lines for the case of compliant micro-constriction. As reported in our
17 previous work, from atomic force microscopy data[8], HeLa cell lines are stiffer ($E_c = 13\ 532 \pm 1623\ Pa$) than MDA-MB-

1 231 ($E_c = 1004 \pm 100\ Pa$). Fig. 5(a) shows the comparison of entry time between HeLa and MDA-MB-231 cell line for
2 compliant micro-constriction (f_{p1}). We observe a further decrement in the entry time of cell with the decrease in the cell
3 stiffness. At $\rho = 1.64$, the entry time for MDA-MB-231 cell line is smaller than HeLa cell line by more than one fourth,
4 which is quite significant. Thus, we conclude, the entry time is dependent on stiffness of compliant microchannel wall as
5 well as the cell. This has also been confirmed by the correlation we have developed as shown in eqn. 6 of the main
6 manuscript.
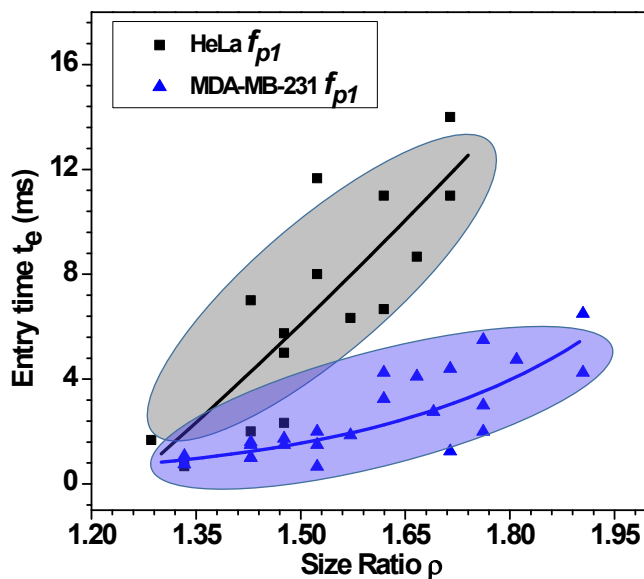
7

8 **Fig. S5** Variation of entry time with the Young's modulus value of the cell line; HeLa cell ($E_c = 13\ 532 \pm 1623\ Pa$) and
9 MDA-MB-231 ($E_c = 1004 \pm 100\ Pa$)[6], a decrement in the Young's modulus of the cell further increases the speed of cell
10 entry into the compliant micro-constriction, applied pressure across the channel was $100\ mbar$.

11 **References**

12 1   Z. S. Khan, N. Kamyabi, F. Hussain and S. A. Vanapalli, *Converg. Sci. Phys. Oncol.*, 2017, **3**, 024001.

13 2   H. Bruus, *oxford Univ. Press. New York.*

14 3   P. Sajeesh, M. Doble and A. K. Sen, *Biomicrofluidics*, 2014, **8**, 1–23.

15 4   A. Raj, R. Halder, P. Sajeesh and A. K. Sen, *Microfluid. Nanofluidics*, 2016, **20**, 1–16.

16 5   A. P. Ebrahimi, *J. Vasc. Interv. Neurol.*, 2009, **2**, 155–162.

17 6   A. Raj and A. K. Sen, *Microfluid. Nanofluidics*, 2016, **20:31**, 1–13.

18 7   S. H. Au, B. D. Storey, J. C. Moore, Q. Tang, Y.-L. Chen, S. Javaid, A. F. Sarioglu, R. Sullivan, M. W. Madden, R.
19   O'Keefe, D. A. Haber, S. Maheswaran, D. M. Langenau, S. L. Stott and M. Toner, *Proc. Natl. Acad. Sci.*, 2016,
20   **113**, 4947–4952.

21 8   P. Sajeesh, A. Raj, M. Doble and A. K. Sen, *RSC Adv.*, 2016, **6**, 74704–74714.

22

23

1